Houlsby, G. T. & Withers, N. J. (1988). *Géotechnique* **38,** No. 4, 575–587

Analysis of the cone pressuremeter test in clay

G. T. HOULSBY* and N. J. WITHERS†

The cone pressuremeter test is a new in situ test which combines a standard cone penetrometer with a pressuremeter. An analysis of the cone pressuremeter test in clay is presented. The analysis shows that important information about soil properties can be gained from the unloading section of the pressuremeter curve, as well as the loading section. Seven tests using a prototype cone pressuremeter are analysed using the new method, and the derived soil parameters are compared with other tests at the same site. The analysis is shown to fit closely the behaviour observed in the tests, and the derived values of shear modulus and undrained strength agree well with the results of other tests.

KEYWORDS: **analysis; clays; shear modulus; shear strength; site investigation; soil properties.**

Le nouvel essai au pressiomètre à cône combine un pénétromètre à cône de type standard avec un pressiomètre. L'article présente une analyse de l'essai au pressiomètre à cône dans l'argile. L'analyse démontre que des indications importantes au sujet des propriétés du sol peuvent s'acquérir à partir des zones de déchargement et de chargement de la courbe de pressiomètre. Sept essais employant un pressiomètre à cône prototype sont analysés par la nouvelle méthode et les paramètres de sol calculés sont comparés avec d'autres essais au même emplacement. On démontre que l'analyse correspond bien au comportement observé au cours des essais et que les valeurs calculées du module de cisaillement et de la résistance dans l'état non-drainé s'accordent bien avec les résultats d'autres essais.

NOTATION

A, B	constants of integration
E	Young's modulus
f	factor (*see* equation (43))
f_s	sleeve friction
G	shear modulus
I_r	rigidity index: G/s_u
m	factor ($m = 1$ for cylindrical, $m = 2$ for spherical)
p_a	atmospheric pressure
q_c	cone tip resistance
r	radial co-ordinate
r_{cc}, r_{ce}, r_{ee}	radii (*see* Fig. 1)
R	pressuremeter radius
R_c	pressuremeter radius during contraction
R_e	pressuremeter radius at maximum expansion
R_i	initial pressuremeter radius
s	$(\sigma_r + \sigma_\theta)/2$
s_u	undrained shear strength
t	$(\sigma_r - \sigma_\theta)/2$
u	pore water pressure
u_0	in situ pore water pressure
ε	pressuremeter strain
ε_e	pressuremeter strain at maximum expansion
ε_θ, ε_r, ε_z	hoop, radial and axial strain
ν	Poisson's ratio
σ_θ, σ_r, σ_z	hoop, radial and axial stress
ψ	pressuremeter pressure
ψ_e	expansion limit pressure
ξ	radial displacement

INTRODUCTION

The cone pressuremeter is a new in situ testing device which combines a 60° electric piezocone with the pressuremeter test (Withers, Schaap & Dalton, 1986). The pressuremeter is of the same diameter as the cone, and is mounted on the penetrometer shaft a short distance behind the cone unit. The main reasons for the development of the new test are detailed below.

The cone penetration test is now well-established as a simple and relatively economical test which is of particular value in making detailed profiles of soil properties. By using friction ratio measurements, as well as pore pressure measurements in the case of the piezocone, reasonably reliable classification of soils can be achieved. Absolute values of cone resistance can be used to estimate strength parameters in either

Discussion on this Paper closes on 1 April, 1989. For further details, see p. ii.

* Oxford University.

† Dawson Offshore, Perth; formerly with Fugro Geotechnical Engineers, Leidschendam, Holland.

sands or clays. The cone gives, however, only a poor indication of soil stiffness.

The pressuremeter, on the other hand, is a device well-suited to measuring both soil stiffness and strength parameters. Most research has concentrated on the development of the self-boring pressuremeter, in which the aim is to install the pressuremeter in the ground with minimal disturbance. Unfortunately, this ideal is on occasions difficult to achieve. Although the highest quality pressuremeter results may be achieved using the self-boring technique, a possible alternative is to allow a repeatable amount of ground disturbance prior to the pressuremeter test. The installation of the pressuremeter behind a solid tip which is driven or pushed into the ground should result in such a repeatable amount of disturbance. This type of pressuremeter will be described as a full-displacement device as compared to the self-boring machine. The combination of the profiling ability of the piezocone with friction sleeve, together with the stress–strain measurements from the pressuremeter, in the form of the cone pressuremeter is a particular form of the full-displacement type. Another earlier example is the LPC pressiopenetrometer developed by Jezequel, Lamy & Perrier (1982).

The new test is thus intended to combine some of the merits of the pressuremeter test with the operational convenience of the cone penetration test, and in particular the new test allows the possibility of making accurate soil stiffness and strength measurements.

This Paper introduces an analytical method to derive the undrained shear strength and shear modulus from full-displacement pressuremeter test data in clays. The values so obtained from tests (made with a prototype pressuremeter developed by Fugro) in overconsolidated Gault clay at Madingley, Cambridge, are compared with values obtained from self-boring pressuremeter, screw plate vane and triaxial tests. Possible ways to develop more complete analyses of full-displacement pressuremeter data are then discussed in the light of the form of the pressure–expansion–contraction curves obtained at Madingley.

ANALYTICAL METHOD

Existing published use of full-displacement pressuremeter data has been confined to the empirical transformation of the expansion curve into a p–y curve for laterally loaded driven piles. This empirical use has been validated by field tests (Brown, 1985; Robertson, Hughes, Campanella & Sy, 1983; Robertson, Hughes, Campanella, Brown & McKeown, 1986). Fundamental soil parameters need also to be derived from the tests if the cone pressuremeter is to become widely accepted and applied. This requires an analysis which explains the pressure–expansion–contraction curve.

The initial installation of the full-displacement pressuremeter is modelled theoretically as the expansion of a cylindrical cavity within the soil. The expansion phase of the pressuremeter test is modelled as a continued expansion of the same cylindrical cavity, and the contraction phase as a cylindrical contraction. This modelling of the installation will be somewhat in error, as the penetration of a rod tipped by a 60° cone involves different stress paths from the cavity expansion. Cylindrical cavity expansion theory has, however, been used with some success to model installation of penetrometers and piles (e.g. Randolph, Carter & Wroth, 1979). It can be shown theoretically that the cylindrical cavity expansion theory models correctly the penetration of a cone with a very small tip angle, but is approximate for the 60° cone tip (Norbury and Wheeler, 1987). Baligh (1986) discussed in detail the importance of modelling the correct strain paths for soil elements, and Teh (1987) implemented Baligh's strain path method for the analysis of the 60° cone (*see also* Teh & Houlsby, 1988). Teh's analysis shows that the stress distribution far behind the cone tip is similar to the distribution created by the expansion of a cylindrical cavity from zero initial radius. The use of the simpler cylindrical cavity expansion theory is therefore justified, provided that the bottom of the pressuremeter section is located more than about 10 diameters behind the cone tip.

Errors in the modelling of the expansion and contraction phases of the test by cylindrical theory are also due to the finite length of the pressuremeter, and with the length/diameter ratio of 10 used for the prototype device, these may be expected to be relatively small. At large strains, however, the boundary between the elastically and plastically deforming soil regions has a diameter comparable to the length of the pressuremeter. Under these circumstances, it is debatable as to whether a spherical cavity expansion theory may be more appropriate for modelling the test. In the following analysis the solutions for both the cylindrical and spherical cases are developed together, so that a comparison may be made between the two interpretations.

During the installation of the cone, a cavity of zero initial diameter is expanded to a finite size, and during the pressuremeter expansion a further 50% increase in radius is possible using the prototype device. It is therefore necessary to analyse the pressuremeter using large strain

theory. It will also be necessary in the following analysis to keep careful track of the radii of material points within the soil at different stages of the test.

The analysis is carried out in terms of total stresses, since the problem is treated as undrained. Compressive stresses and strains are defined as positive. The clay is modelled as an incompressible linear elastic, perfectly plastic (Tresca) material. As the ratio of shear stiffness to strength $G/s_u = I_r$ of the clay will typically be large (i.e. greater than 30) it follows that the strain to the initiation of plasticity is small. A small strain solution will therefore be adopted for the elastic region (resulting in a considerable economy in the mathematics). The combination of large strain analysis in the plastically deforming region with small strain in the elastic region was used by Gibson & Anderson (1961).

The stages of the pressuremeter test are shown in Fig. 1, in which the positions of three material points are traced. Point A is initially on the centre-line of the pressuremeter before installation (Fig. 1(a)). After installation A is at a radius R_i; the pressuremeter radius (Fig. 1(b)). The pressuremeter is then expanded to its maximum dimension R_e (Fig. 1(c)) and finally Fig 1 (c) shows A at radius R_c ($R_i < R_c < R_e$) during the contraction phase.

Point E lies on the elastic-plastic boundary at the maximum expansion (Fig. 1(c)) and is then at radius r_{ee}; initially point E was at r_{eo}. Point C lies within the plastic region at radius r_{ce} at the stage of maximum pressuremeter expansion, and lies on the elastic-plastic boundary at radius r_{cc} when the pressuremeter has been contracted to dimension R_c.

After pressuremeter expansion (Fig. 1(c)) the material between A and E has been deformed plastically, whilst the material outside E is still elastic. After contraction (Fig. 1(d)) the material outside E has remained elastic, that between C and E has been loaded plastically and unloaded elastically, and the material between A and C has been loaded plastically, and then unloaded sufficiently so that reverse plasticity has occurred.

It is useful to show the positions of the stress points for different materials on a plot of shear stress $t = (\sigma_r - \sigma_\theta)/2$ against normal stress $s = (\sigma_r + \sigma_\theta)/2$. This is demonstrated in Fig. 2 for the cylindrical expansion case. Fig. 2(a) shows the stress states at maximum expansion. All the material inside E is deforming plastically, whilst the material outside E remains elastic. During elastic behaviour s remains constant and during plastic behaviour t remains constant.

On contraction the stress points move to the positions shown in Fig. 2(b). All the points first unload elastically, and then those inside C unload plastically. It is the tracing of the complete stress

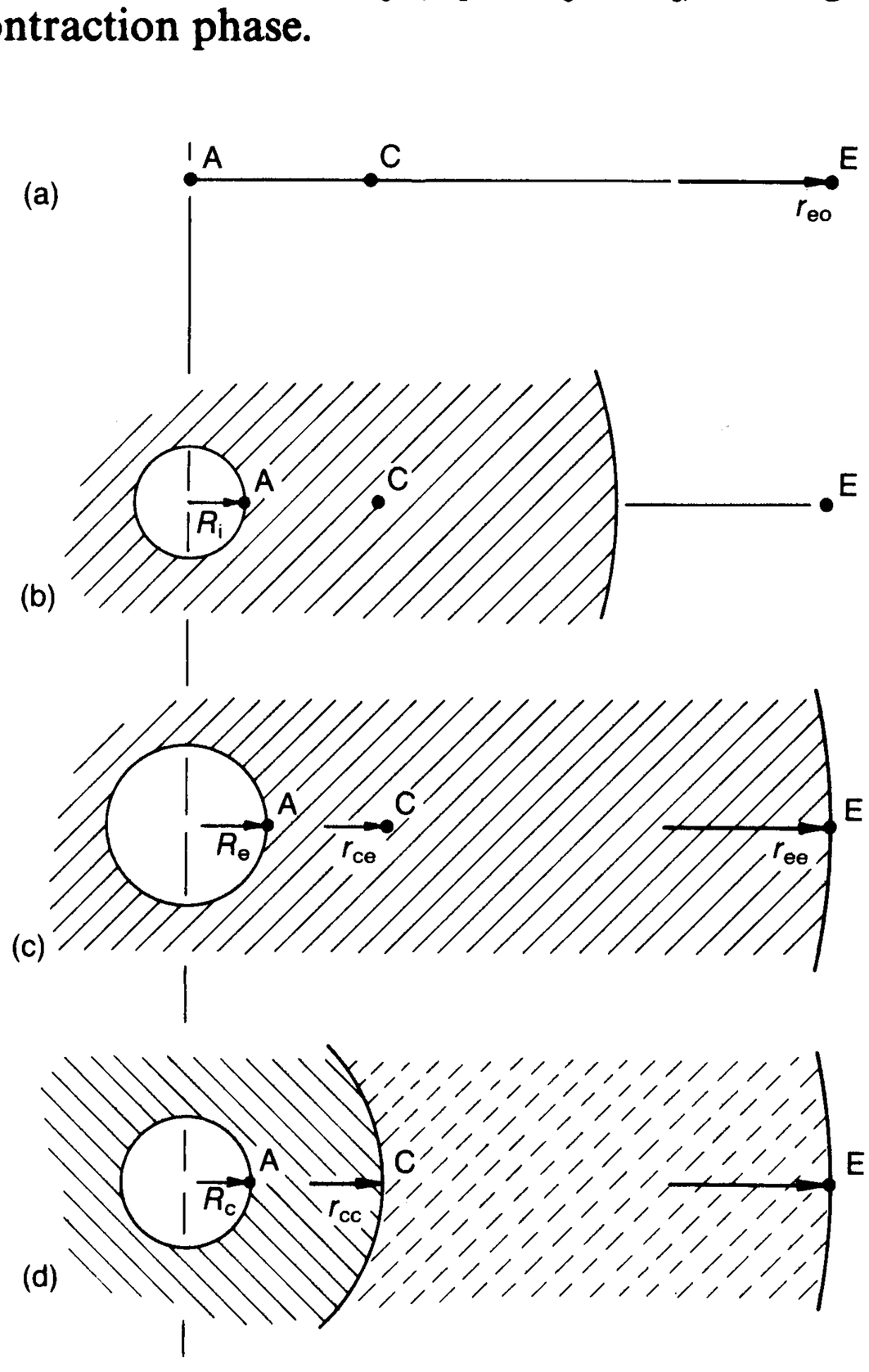

Fig. 1. Definitions of radii used in analysis: (a) in situ conditions; (b) after pressuremeter installation; (c) at maximum pressuremeter expansion; (d) during pressuremeter contraction

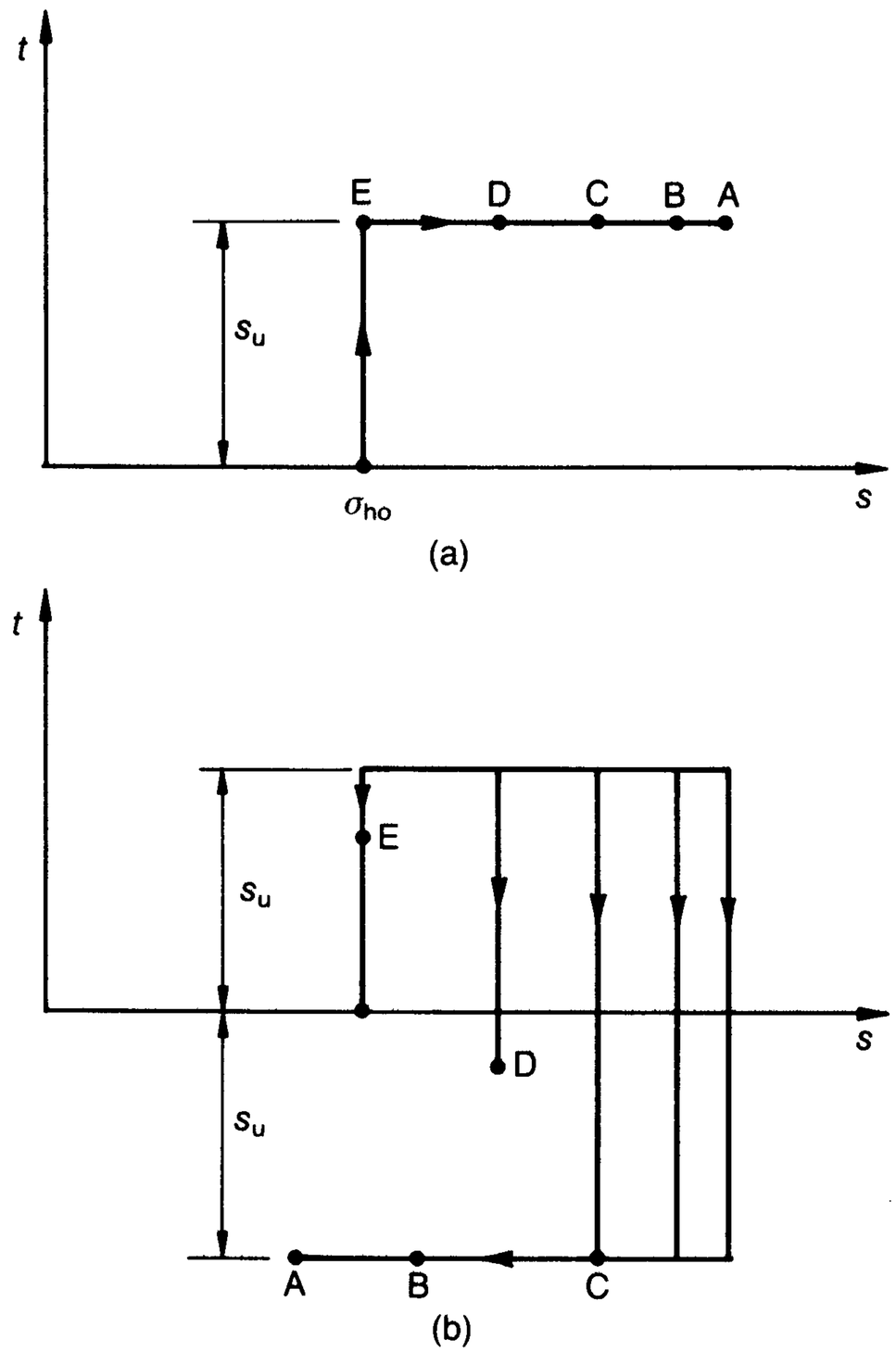

Fig. 2. Stress states around the cone pressuremeter: (a) at maximum expansion; (b) during contraction

paths, including unloading from different stress points, which is the key to the analysis of the contraction.

Pressuremeter terminology

Data from pressuremeter tests are conventionally presented in terms of the pressuremeter inflation pressure ψ and either the change of volume of the pressuremeter, or the hoop strain at the pressuremeter surface ε (by convention this strain only is defined as tensile positive to avoid a minus sign which would otherwise appear in the results, i.e. $\varepsilon = -\varepsilon_\theta$ at the pressuremeter surface). In this Paper, the hoop strain has been adopted as the preferred parameter. In the small strain analysis which is usually applied, it is not necessary to distinguish between the various possible definitions of strain, e.g. the Cauchy strain $(R - R_i)/R_i$ and the Hencky (logarithmic or natural) strain $\ln(R/R_i)$, as they reduce to the same value for small strains. In the large strain analysis presented here, such a distinction is necessary, and the Hencky strain is chosen as it simplifies the mathematical treatment.

Small strain elastic analysis

An essential preliminary to the pressuremeter analysis is the analysis for stresses and strains in the region in which the soil remains elastic. For simplicity the elastic analysis will be carried out in terms of small strains only, which is reasonable provided that the factor G/s_u is large. The results of the analysis are well-known, but the essential details are repeated here for completeness. For simplicity of notation, the calculation is presented in terms of total stresses and strains, but is of course applicable to stress and strain increments.

Let the radial co-ordinate be r and radial displacement be ξ. The definitions of radial and hoop strain are therefore (taking compression positive)

$$\varepsilon_r = -\frac{d\xi}{dr} \tag{1}$$

$$\varepsilon_\theta = -\frac{\xi}{r} \tag{2}$$

In the spherical case, the two hoop strains (and stresses) are equal, and in the plane strain cylindrical case the axial strain ε_z is zero, resulting in the relationship between stresses

$$\sigma_z = \nu(\sigma_r + \sigma_\theta) \tag{3}$$

Thus the elastic stress–strain relationships for the spherical case may be written

$$E\begin{bmatrix}\varepsilon_r\\ \varepsilon_\theta\end{bmatrix} = \begin{bmatrix}1 & -2\nu\\ -\nu & 1-\nu\end{bmatrix}\begin{bmatrix}\sigma_r\\ \sigma_\theta\end{bmatrix} \tag{4}$$

and in the cylindrical case

$$E\begin{bmatrix}\varepsilon_r\\ \varepsilon_\theta\end{bmatrix} = \begin{bmatrix}1-\nu^2 & -\nu-\nu^2\\ -\nu-\nu^2 & 1-\nu^2\end{bmatrix}\begin{bmatrix}\sigma_r\\ \sigma_\theta\end{bmatrix} \tag{5}$$

The inverses of these equations may readily be obtained. For the spherical case

$$\begin{bmatrix}\sigma_r\\ \sigma_\theta\end{bmatrix} = \frac{E}{(1+\nu)(1-2\nu)}\begin{bmatrix}1-\nu & 2\nu\\ \nu & 1\end{bmatrix}\begin{bmatrix}\varepsilon_r\\ \varepsilon_\theta\end{bmatrix} \tag{6}$$

and for the cylindrical case

$$\begin{bmatrix}\sigma_r\\ \sigma_\theta\end{bmatrix} = \frac{E}{(1+\nu)(1-2\nu)}\begin{bmatrix}1-\nu & \nu\\ \nu & 1-\nu\end{bmatrix}\begin{bmatrix}\varepsilon_r\\ \varepsilon_\theta\end{bmatrix} \tag{7}$$

The radial equilibrium equation for the spherical case is

$$\frac{d\sigma_r}{dr} + \frac{2(\sigma_r - \sigma_\theta)}{r} = 0 \tag{8}$$

and for the cylindrical case

$$\frac{d\sigma_r}{dr} + \frac{(\sigma_r - \sigma_\theta)}{r} = 0 \tag{9}$$

The solutions for the spherical and cylindrical cases can be developed together by writing $m = 2$ for the spherical case and $m = 1$ for the cylindrical. Equations (6) and (7) then become

$$\begin{bmatrix}\sigma_r\\ \sigma_\theta\end{bmatrix} = \frac{E}{(1+\nu)(1-2\nu)}\begin{bmatrix}1-\nu & m\nu\\ \nu & 1-(2-m)\nu\end{bmatrix}\begin{bmatrix}\varepsilon_r\\ \varepsilon_\theta\end{bmatrix} \tag{10}$$

and equations (8) and (9) become

$$\frac{d\sigma_r}{dr} + \frac{m(\sigma_r - \sigma_\theta)}{r} = 0 \tag{11}$$

Substituting equation (10) into (11) gives a differential equation in terms of strains, and further substituting the definitions (1) and (2) gives a differential equation for ξ. It is remarkable that neither of the material properties E and ν appear in this equation

$$\frac{d^2\xi}{dr^2} + m\frac{d\xi}{dr} - m\frac{\xi}{r} = 0 \tag{12}$$

which has the general solution

$$\xi = Ar + \frac{B}{r^m} \tag{13}$$

where A and B are constants of integration.

For the case of expansion in an infinite material, the displacement at infinity is zero so that $A = 0$. Substitution for the strains and

stresses then gives the solutions

$$\varepsilon_\theta = -\frac{B}{r^{m+1}} \tag{14}$$

$$\varepsilon_r = -m\varepsilon_\theta \tag{15}$$

$$\sigma_\theta = 2G\varepsilon_\theta \tag{16}$$

$$\sigma_r = -2mG\varepsilon_\theta \tag{17}$$

where G is the shear modulus, equal to $E/2(1+v)$.

The solution for plastic expansion is now presented. The solution is well-known (Gibson & Anderson, 1961) and is reproduced here solely as a precursor to the contraction analysis.

Initial yield

The initial stress state in the ground is $\sigma_r = \sigma_\theta = \sigma_{h0}$ (for the spherical analysis it must be assumed that the initial state is one of isotropic stress, i.e. $K_0 = 1{\cdot}0$; the implications of this simplifying assumption are not yet fully explored). Initial yield will occur, assuming the Tresca yield condition, when

$$(\sigma_r - \sigma_\theta) = 2s_u \tag{18}$$

(It must also be assumed in the cylindrical case that the axial stress σ_z is intermediate between σ_r and σ_θ at yield. This will be true for all but very shallow pressuremeter tests.) Applying the above elastic analysis in terms of stress increments, and noting that it implies that $\Delta\sigma_r = -m\Delta\sigma_\theta$, yield will occur in the spherical case when

$$\sigma_r = \sigma_{h0} + \tfrac{4}{3}s_u, \quad \sigma_\theta = \sigma_{h0} - \tfrac{2}{3}s_u \tag{19}$$

and in the cylindrical case when

$$\sigma_r = \sigma_{h0} + s_u, \quad \sigma_\theta = \sigma_{h0} - s_u \tag{20}$$

Equilibrium in the plastic zone

As equation (18) applies throughout the plastic zone, equation (11) can be rewritten

$$\frac{d\sigma_r}{dr} + \frac{2ms_u}{r} = 0 \tag{21}$$

which has solution

$$\sigma_r + 2ms_u \ln(r) = A \tag{22}$$

where A is a constant of integration. This can be used to relate the stresses at two different radii

$$\sigma_{r2} = \sigma_{r1} + 2ms_u \ln\left[\frac{r_1}{r_2}\right] \tag{23}$$

and in particular

$$\psi = \sigma_{r1} + 2ms_u \ln\left[\frac{r_1}{R_e}\right] \tag{24}$$

where ψ is the pressuremeter expansion pressure.

Strains and compatibility

Noting from equations (19) and (20) that the increment in radial stress at the initiation of plasticity can be expressed as $s_u(2+m)/3$ it follows from equation (17) that the hoop strain $\varepsilon_{\theta e}$ at the elastic-plastic boundary radius r_{ee} (*see* point E in Fig. 1(c)) is $-s_u(2+m)/6mG$. Writing G/s_u as I_r, the rigidity index (after Vesic, 1963) and noting that for either $m=1$ or $m=2$ the factor $6m/(2+m)$ is also equal to $(m+1)$, the hoop strain is equal to $-1/I_r(m+1)$.

The installation and subsequent expansion of the full-displacement pressuremeter is modelled as the expansion of a cavity from zero initial radius (Fig. 1). The compatibility condition of no change of volume of material between A and E requires that

$$r_{e0}^{m+1} = r_{ee}^{m+1} - R_e^{m+1} \tag{25}$$

Thus

$$\left[\frac{R_e}{r_{ee}}\right]^{m+1} = 1 - \left[\frac{r_{e0}}{r_{ee}}\right]^{m+1} \tag{26}$$

Using the Hencky definition of hoop strain gives $\varepsilon_{\theta e} = \ln[r_{e0}/r_{ee}]$ so that

$$\left[\frac{R_e}{r_{ee}}\right]^{m+1} = 1 - \exp[(m+1)\varepsilon_{\theta e}] \tag{27}$$

and assuming $\varepsilon_{\theta e}$ is small (as already discussed) this simplifies to

$$\left[\frac{R_e}{r_{ee}}\right]^{m+1} = -(m+1)\varepsilon_{\theta e} = \frac{1}{I_r} \tag{28}$$

Denoting the radial stress at the pressuremeter surface R_e during expansion by ψ_e, and noting that the value of the radial stress at r_{ee} is $\sigma_{h0} + [(2+m)/3]s_u$, equations (24) and (28) may be combined to give

$$\psi_e = \sigma_{h0} + \frac{(2+m)}{3}s_u + \frac{2m}{(m+1)}s_u \ln(I_r) \tag{29}$$

This may be further simplified by noting that for both $m=1$ and $m=2$, $2m/(m+1) = (2+m)/3$, so that

$$\psi_e = \sigma_{h0} + \frac{(2+m)}{3}s_u[1 + \ln(I_r)] \tag{30}$$

This well-known result for cavity expansion from zero initial radius applies at all values of pressuremeter expansion, so that the expansion phase is expected to take place at constant pressure. This constant pressure is also known as the limit pressure for the expansion of a finite cavity (Gibson & Anderson, 1961).

A further important result of this analysis is that the ratio of the elastic-plastic radius r_{ee} to the pressuremeter radius R_e is given by $I_r^{[1/(m+1)]}$.

This is the well-known result that the ratio of the radius of the elastic-plastic boundary to the cavity radius is $I_r^{(1/2)}$ for cylindrical expansion and $I_r^{(1/3)}$ for spherical expansion.

Cavity contraction

During the initial phase of cavity contraction, the whole of the soil behaves elastically, with elastic unloading of the previously plastic section. The elastic phase ends when the condition for reverse plasticity

$$\sigma_r - \sigma_\theta = -2s_u \tag{31}$$

is satisfied at the surface of the pressuremeter. Noting the ratios of changes of hoop and radial strains (equations (16) and (17)) this will occur when the pressure at the pressuremeter surface has reduced from ψ_e to $\psi_e - 2s_u(2 + m)/3$.

If the maximum pressuremeter strain (defined as the negative hoop strain at the pressuremeter surface) is ε_e, then the strain at the initiation of reverse plasticity is $\varepsilon_e - s_u(2 + m)/3mG$ which is also equal to $\varepsilon_e - 2/I_r(m + 1)$. The slope of the elastic section of the pressuremeter stress–strain curve is $2mG$.

On further unloading, a zone of soil in which reversed plasticity occurs spreads outwards from the pressuremeter. Within this region the equilibrium condition results in equations similar to (21)–(23), except that the sign of s_u is changed, so that

$$\sigma_{r_2} = \sigma_{r_1} - 2ms_u \ln\left[\frac{r_1}{r_2}\right] \tag{32}$$

The radial stress at material point C at the stage of maximum pressuremeter expansion (Fig. 1(c)) is given (from equation (24)) by the expression $\psi_e - 2ms_u \ln [r_{ce}/R_e]$ and this will then reduce elastically until the reverse elastic-plastic boundary just reaches C (Fig. 1(d)) at which stage the radial stress at point C will be

$$\psi_e - \frac{2(2 + m)}{3} s_u - 2ms_u \ln\left[\frac{r_{ce}}{R_e}\right]$$

Using equation (32) then yields the current value of the pressuremeter pressure

$$\psi = \psi_e - \frac{2(2 + m)}{3} s_u - 2ms_u \ln\left[\frac{r_{ce}}{R_e}\right] - 2ms_u \ln\left[\frac{r_{cc}}{R_c}\right] \tag{33}$$

The compatibility condition of no change of volume of material between A and C gives

$$r_{ce}^{m+1} - R_e^{m+1} = r_{cc}^{m+1} - R_c^{m+1} \tag{34}$$

which can be arranged as

$$\left[\frac{r_{ce}}{r_{cc}}\right]^{m+1} - 1 = \left[\frac{R_c}{r_{cc}}\right]^{m+1} \left\{\left[\frac{R_e}{R_c}\right]^{m+1} - 1\right\} \tag{35}$$

The change of hoop strain during unloading of point C from plastic loading to plastic unloading gives

$$\frac{2}{(m + 1)} \frac{1}{I_r} = \ln\left[\frac{r_{ce}}{r_{cc}}\right] \tag{36}$$

and the definition of logarithmic pressuremeter strain gives

$$\varepsilon_e - \varepsilon = \ln\left[\frac{R_e}{R_c}\right] \tag{37}$$

Substituting equations (36) and (37) into (35) leads to

$$\exp(2/I_r) - 1 = \left[\frac{R_c}{r_{cc}}\right]^{m+1} [\exp\{(m + 1)(\varepsilon_e - \varepsilon)\} - 1] \tag{38}$$

or

$$(m + 1) \ln\left[\frac{R_c}{r_{cc}}\right] = -\ln\left[\frac{\exp\{(m + 1)(\varepsilon_e - \varepsilon)\} - 1}{\exp(2/I_r) - 1}\right] \tag{39}$$

Equation (33) may be re-arranged as

$$\psi = \psi_e - \frac{2(2 + m)}{3} s_u + 2ms_u \left\{2 \ln\left[\frac{R_c}{r_{cc}}\right] + \ln\left[\frac{R_e}{R_c}\right] + \ln\left[\frac{r_{cc}}{r_{ce}}\right]\right\} \tag{40}$$

and substitution of equations (36)–(38) leads (after some manipulation) to

$$\psi = \psi_e - \frac{2(2 + m)}{3} s_u \left\{1 + \frac{1}{I_r} - \frac{(m + 1)}{2}(\varepsilon_e - \varepsilon) + \ln\left[\frac{\exp\{(m + 1)(\varepsilon_e - \varepsilon)\} - 1}{\exp(2/I_r) - 1}\right]\right\} \tag{41}$$

which in turn may be simplified to

$$\psi = \psi_e - \frac{2(2 + m)}{3} s_u \times \left\{1 + \ln\left(\sinh\left[\frac{(m + 1)}{2}(\varepsilon_e - \varepsilon)\right]\right) - \ln\left(\sinh\left[\frac{1}{I_r}\right]\right)\right\} \tag{42}$$

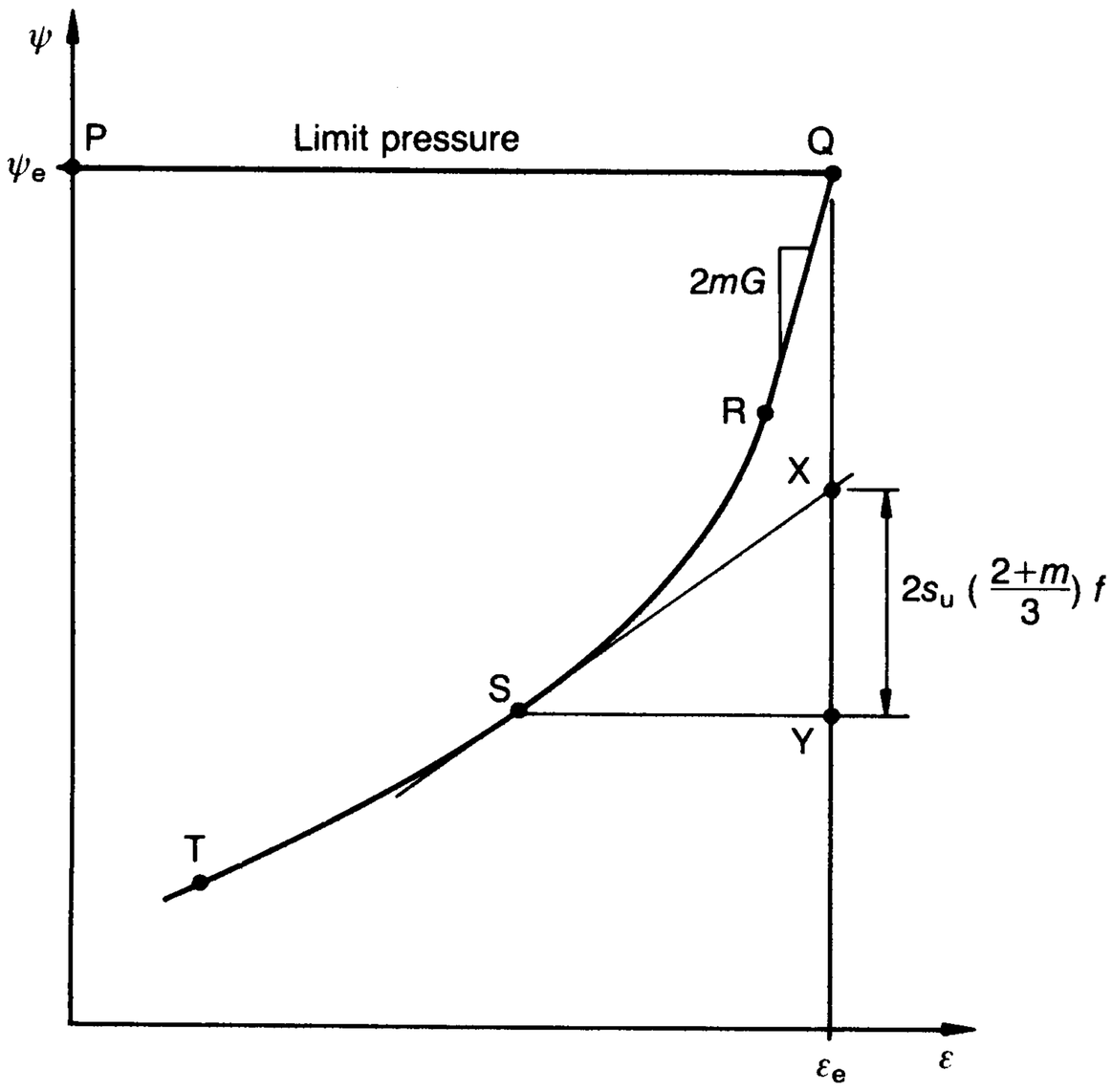

Fig. 3. Constructions to determine G and s_u

This solution applies until point C coincides with point E, at which stage a limiting pressure in cavity contraction would be reached. In practice this would involve such a high value of $\varepsilon_e - \varepsilon$ (i.e. of the ratio R_e/R_c) that this condition will not be attained with realistic pressuremeter geometries.

The shear modulus G and the undrained shear strength s_u may be readily obtained by simple geometric constructions based on the pressuremeter unloading curve. Firstly the shear modulus is obtained from the initial slope of the unloading curve (QR in Fig. 3) which is of slope $2mG$. Although s_u could in principle be derived from the value of $(\psi_e - \psi)$ at the end of the linear elastic unloading, which is given by $2s_u(2 + m)/3$, the point at which linearity ends will be difficult to determine accurately from test data. More useful is the simple construction shown in Fig. 3 in which SX is a tangent to the unloading curve at S, which can be compared with the construction used for the loading curve proposed separately by Palmer (1972); Baguelin, Jezequel, Lemee & Le Mehaute (1972); and Ladanyi (1972). The intercept XY in Fig. 3 is given by

$$(\varepsilon_e - \varepsilon)\frac{d\psi}{d\varepsilon} = f\,\frac{2(2+m)}{3}\,s_u \qquad (43)$$

where f is a function purely of $(m + 1)(\varepsilon_e - \varepsilon)/2$

$$f = \frac{\dfrac{(m+1)}{2}(\varepsilon_e - \varepsilon)}{\tanh\left[\dfrac{(m+1)}{2}(\varepsilon_e - \varepsilon)\right]} \qquad (43)$$

The value of f is near unity for all realistic values of $(m + 1)(\varepsilon_e - \varepsilon)/2$ and is shown in Table 1.

Table 1. Values of function f

$\frac{(m+1)}{2}(\varepsilon_e - \varepsilon)$	f
0·0	1·000
0·1	1·003
0·2	1·013
0·3	1·030
0·4	1.052
0·5	1·082
0·6	1·117

The above construction can therefore be used to obtain a quick estimate of s_u with the correcting factors in Table 1 only being necessary when attempting to obtain the maximum accuracy from test data.

Having determined G and s_u, the factor I_r is found, and σ_{h0} may then be estimated from the expansion pressure ψ_e and use of equation (30). (The equation of the contraction curve does not depend at all on the value of σ_{h0}, a result also found for the small strain unloading of a pressuremeter in sand (Houlsby, Clarke & Wroth, 1986).)

An alternative construction, based on the fact that $\sinh(x) \simeq x$ for small values of x, and related to the fact that f is near unity, is shown in Fig. 4. The pressure ψ is plotted against $-\ln[\{(m + 1)/2\}(\varepsilon_e - \varepsilon)]$. The expansion limit pressure can as easily be obtained from this plot as from Fig. 3. The advantage is that the slope of the unloading curve is $2s_u(2 + m)/3$ (c.f. the logarithmic plot for loading suggested by Gibson

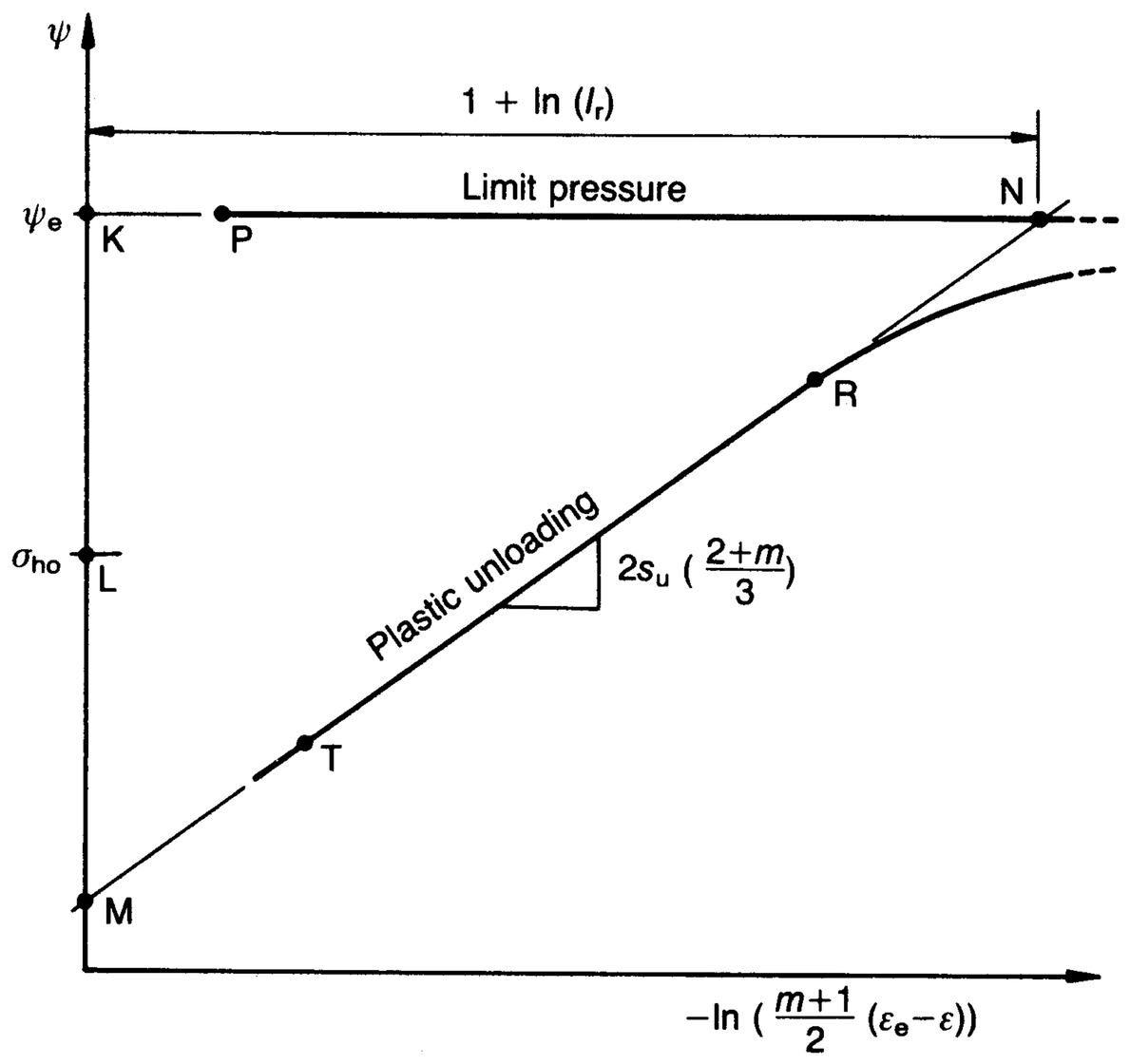

Fig. 4. Logarithmic plot for determination of G, s_u and σ_{h0}

& Anderson (1961)). The abscissa of the intersection of the limit pressure and the plastic unloading line (point N) is used to determine I_r (and hence G) and the value of σ_{h0} is given in theory by the ordinate of point L, the midpoint of KLM. (This last procedure does not, however, seem to give reliable horizontal stress values.) This construction allows straightforward and rapid determination of s_u and G, but usually necessitates computerized replotting of the data.

To summarize the results for the cylindrical (plane strain) analysis

(*a*) the expansion occurs at constant pressure $\psi_e = \sigma_{h0} + s_u(1 + \ln I_r)$
(*b*) initial unloading is at slope $2G$ from (ψ_e, ε_e) to $(\psi_e - 2s_u, \varepsilon_e - 1/I_r)$
(*c*) plastic unloading occurs along the curve

$$\psi = \psi_e - 2s_u\left\{1 + \ln\left(\sinh\left[\varepsilon_e - \varepsilon\right]\right) - \ln\left(\sinh\left[\frac{1}{I_r}\right]\right)\right\} \quad (44)$$

The results for the spherical analysis can be obtained from the plane strain analysis by

(*a*) scaling all stresses (except σ_{h0}) by a factor of $\frac{4}{3}$
(*b*) scaling all strains by a factor $\frac{2}{3}$.

These two scalings have the effect that all stiffnesses are scaled by a factor of 2.

Limit values on contraction pressure

The above analysis, for realistic material parameters and pressuremeter strains, predicts very low, even tensile, radial stresses at the end of the contraction phase. These values will not be measured by the pressuremeter device as, at a certain pressure, the pressuremeter will lose contact with the soil and will register thereafter a constant pressure. Depending on the ground conditions there are three possible values of this cut-off pressure.

(*a*) If the test is in a saturated clay with relatively permeable fissures, or there is any other open channel connected to the water table, then the lowest pressure registered by the device is likely to be the in situ ground water pressure u_0.
(*b*) If these conditions do not apply but (in the case of an onshore test) there is some open channel (e.g. along the cone rods) back to the surface, then the lowest pressure registered may be atmospheric pressure (zero, since it is conventionally taken as the reference point for pressure measurements).
(*c*) If none of these conditions apply, then the lowest expected pressure would be one negative atmosphere $(-p_a)$ representing a zero absolute pressure, at which stage cavitation around the pressuremeter would be expected.

FIELD TESTING

The tests at Madingley, Cambridge, were made with a prototype of the Fugro pressuremeter cone (FPC). This consisted of a pressuremeter mounted above a piezo friction cone of the same diameter (43·7 mm) and 15 cm^2 in area (*see* Fig. 5). The centre of the pressuremeter is 1·5 m above the cone tip. The pressuremeter membrane has a length to diameter ratio of 10. A full description of this prototype can be found in Withers *et al.* (1986).

The prototype was pushed into the ground at 2 cm/s using standard cone rods (10 cm^2 in area). The reduction in area from 15 cm^2 to 10 cm^2 took place 1·07 m above the centre of the pressuremeter. The cone resistance q_c, sleeve friction f_s and pore pressure on the cone face u were measured during penetration.

At the required depth, cone penetration was stopped and a pressuremeter test was performed.

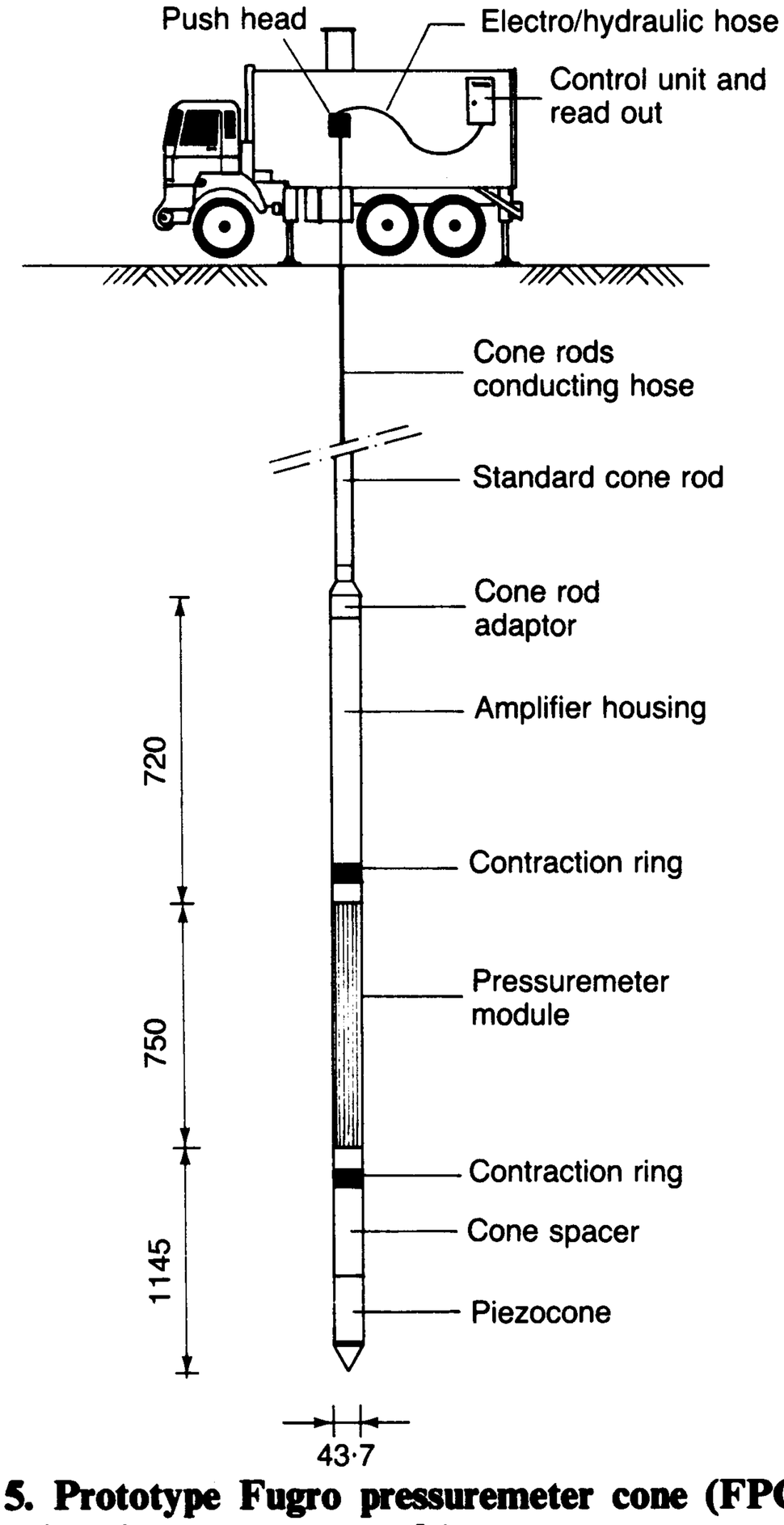

Fig. 5. Prototype Fugro pressuremeter cone (FPC) (all dimensions in mm; not to scale)

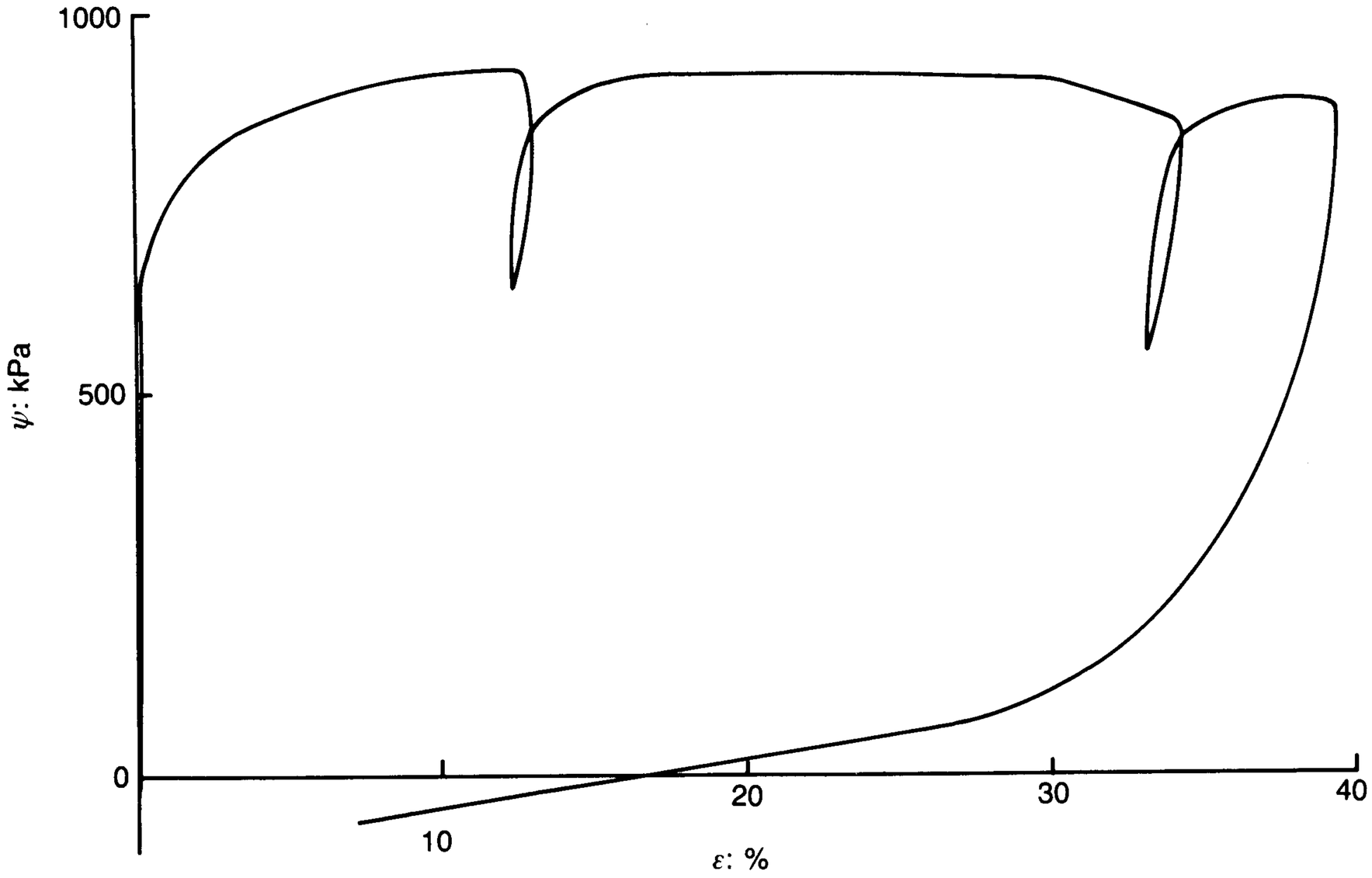

Fig. 6. Pressuremeter expansion–contraction curve for test 15 at 4 m depth

The time between the end of cone penetration and the start of the pressuremeter test varied between 8 and 20 mins. The inflation pressure ψ was measured as were the radial displacements of the membrane ($R - R_i$) at three points separated by 120° at the mid-height.

The choice of strain rate for a pressuremeter test in clay is limited by two factors, both of which can effect the measured soil properties. If the test is too fast, then the strength may be affected by the viscous behaviour of the clay at high strain rate; if it is too slow then partial drainage may occur. The test procedure adopted is necessarily a compromise.

The membrane was inflated at a rate of 5% radial displacement per minute, until one of the strain arms registered an increase of radius of 50%, which is the limit of the pressuremeter. This corresponds to a logarithmic strain ε of approximately 40%. Deflation was then made at 5% per minute. The inflation was interrupted twice to make two small unload–reload loops, after first holding the radial displacement constant for approximately 5–10 mins. The purpose of this was to minimize the apparent hysteresis in the unload–reload loops due to soil creep, and allow a more accurate determination of shear modulus. There is the disadvantage that some partial drainage may have occurred.

A total of six pressuremeter cone tests were made at Madingley in the manner described, in two soundings, at depths of 4·0 m (two tests), 9·0 m, 14·0 m (two tests) and 18·0 m. A seventh test was performed at 4.0 m depth, but for this test, the pressuremeter was mounted behind a long, tapered conical tip with a cone angle of 2° instead of the conventional 60°. In addition, two conventional piezocone soundings were made to a depth of 18·0 m.

A typical pressure–expansion–contraction curve is shown in Fig. 6. The pressure measurements on this curve have been corrected for the stiffness of the membrane by subtraction of a calibration curve obtained from pressuremeter inflation in air. No correction is made for the compliance of the instrument, as this was believed to be of minor importance for testing in these materials. The curve shows a distinct lift-off pressure, followed by a rise over a few percent strain to an almost constant limit pressure. The unloading curve is very similar in character to the curve predicted by the analysis described earlier (the straight line section at the end of the test connects only two data points).

Table 2. Properties derived from tests at Madingley, Cambridge

Test	Depth: m	s_u: kPa	G: MPa	I_r	σ_{h0}: kPa
3	4·0	80	32·8	410	369
5	9·0	150	33·5	223	465
7	14·0	184	68·8	374	461
9	18·0	179	45·6	255	739
15	4·0	111	14·8	133	239
17	14·0	192	49·0	255	641
19	4·0	89	12·1	136	164

ANALYSIS OF TESTS

Using the analysis procedures described above, and assuming that the contraction phase is modelled by the cylindrical case, the parameters given in Table 2 were derived by means of the constructions in Fig. 4. All the results were derived by

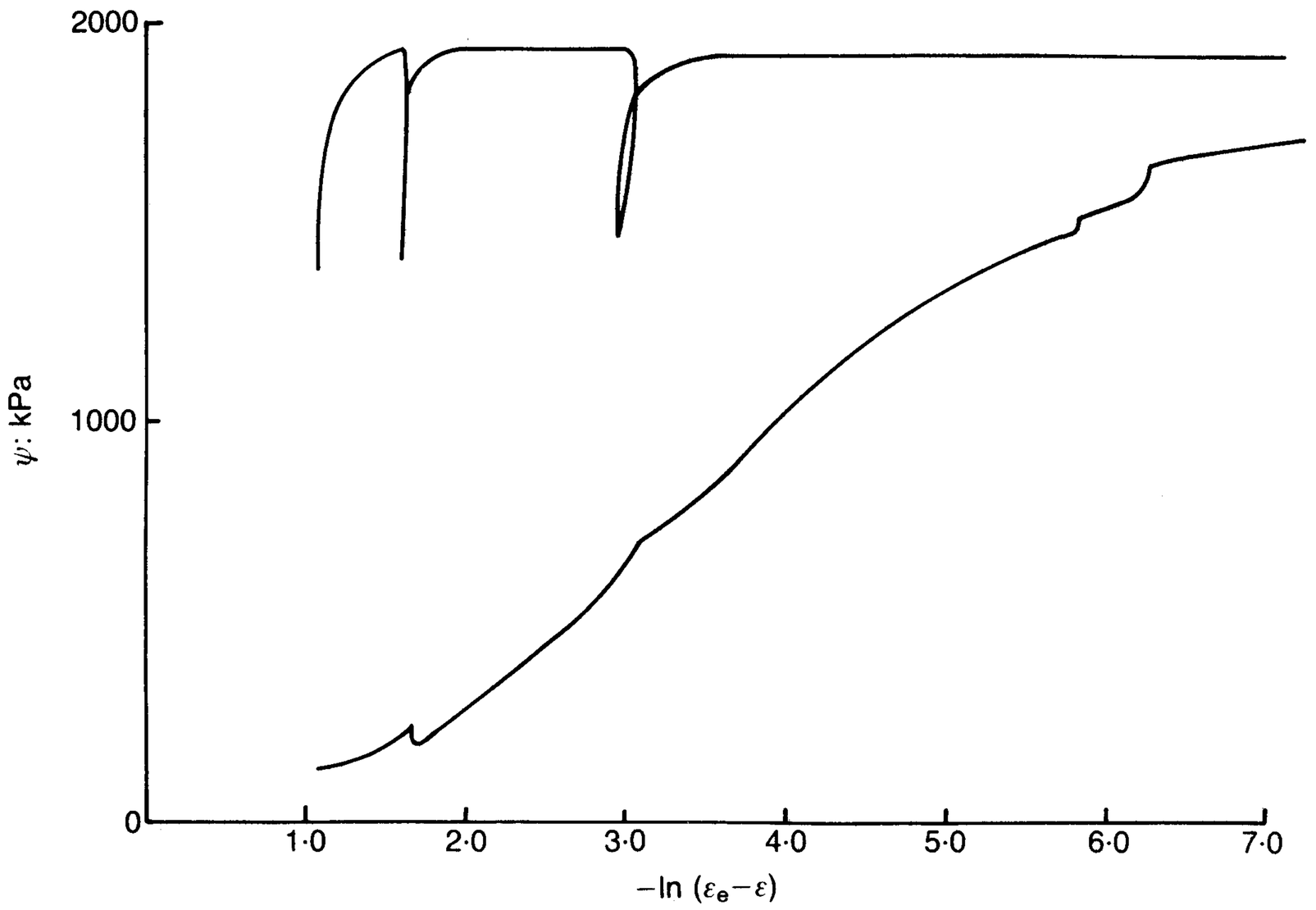

Fig. 7. Pressuremeter expansion–contraction curve on logarithmic plot for test 9 at 18 m depth

using the average strain measurement from the three strain arms, with no use being made of individual strain arm measurements other than to check the consistency of the data. A typical test is shown in this form in Fig. 7. Values of the in situ horizontal stress σ_{h0} have also been estimated, but are not believed to be accurate. In test 19, the penetrometer was tipped by a 2° cone.

From these data the theoretical pressure–expansion–contraction curves can be derived, and Fig. 8 shows the comparison between the analysis and test 5. A limiting pressure on contraction of u_0 has been assumed. The quality of the agreement between the theoretical and observed contraction curve is remarkably good considering the simplified model of soil behaviour which has been used.

The quality of the first set of results with the prototype FPC is high, judged both by the consistent shape of the curves obtained and the numerical values of the parameters derived. The first and third tests gave anomalously high stiffnesses, and this may be related to the fact that, in each of these tests, one of the strain arms exceeded its range, a problem which can be solved by modifying the test procedure. The last test result (with the 2° cone tip) indicated a much lower horizontal stress than other tests.

DISCUSSION OF TEST RESULTS

Undrained shear strength

In Fig. 9 the values of undrained shear strength obtained from the cone pressuremeter are com-

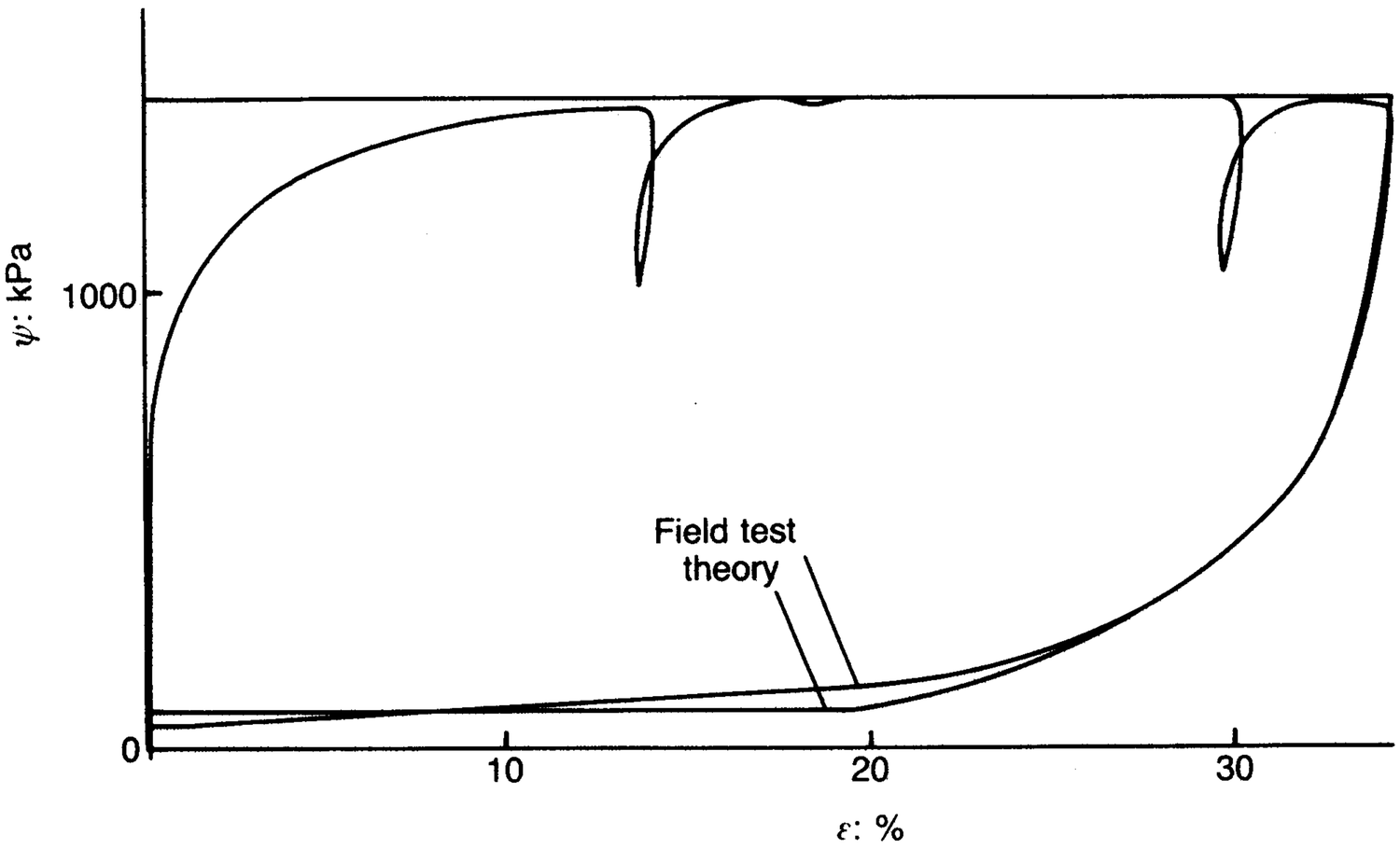

Fig. 8. Comparison of analysis and observed expansion–contraction curve for test 5 at 9 m depth

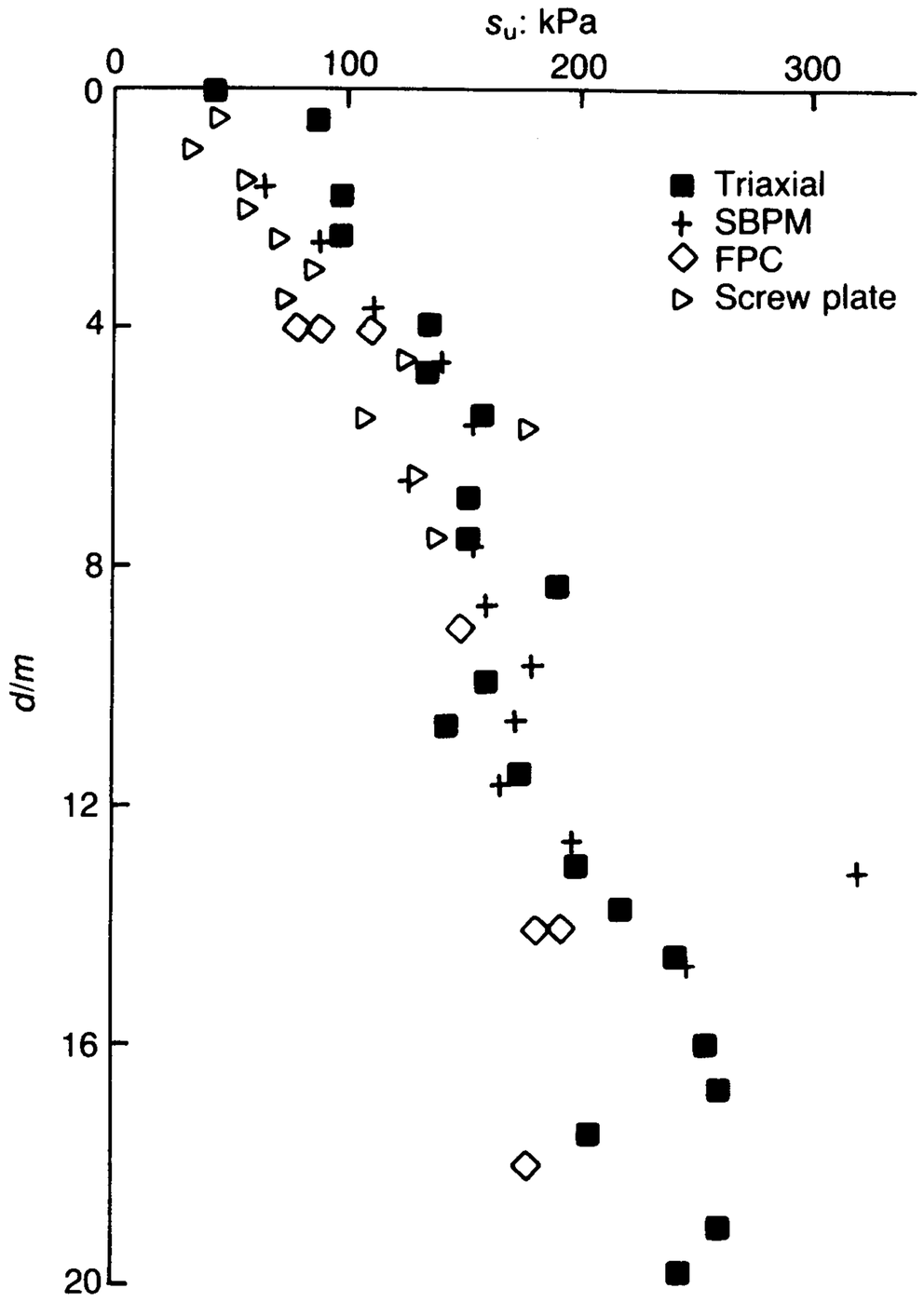

Fig. 9. Comparison of undrained strengths measured by the triaxial, self-boring pressuremeter (SBPM), cone pressuremeter (FPC) and screw plate tests

pared with those obtained from self-boring pressuremeter tests, screw plate tests and triaxial tests in the Gault clay at Madingley (Clarke, 1979; Kay & Parry, 1982; Fugro Ltd, 1979). At each depth, four unconsolidated undrained triaxial tests were carried out, in compression and extension and in each case undisturbed and remoulded. As it is not clear whether the pressuremeter data should be compared with compression or extension triaxial tests, or whether the undisturbed or remoulded case is more appropriate to the cone pressuremeter, the average of the four tests has been plotted at each level.

The values obtained from the cone pressuremeter depend on whether the displacement field around the pressuremeter is assumed to be cylindrical or spherical in form. A detailed discussion of this problem, and its relevance to the estimation of the horizontal stress, is made in a later section. Although spherical cavity expansion theory may be more appropriate for interpretation of the loading phase, the contraction has been modelled by the cylindrical theory. If, alternatively, spherical contraction were to be assumed then the implied s_u values should all be reduced by a factor of 3/4. It can be seen that the cylindrical theory indicates values which agree well with previous measurements, giving values on average only slightly lower than the self-boring pressuremeter and the averaged triaxial results.

There is, of course, no fundamental reason why different tests should yield the same value of the undrained strength, and there is some evidence that pressuremeters give higher strengths than, for example, the vane or triaxial tests (Wroth, 1984). Apart from the observation that the variation of strength with depth measured by the cone pressuremeter agrees closely with that indicated by other devices, more detailed conclusions on the basis of a small number of tests are difficult to draw. For example, the cone pressuremeter tests agree more closely with the undisturbed triaxial tests than with the remoulded values, which for this heavily overconsolidated clay are considerably higher than the undisturbed values.

Shear modulus

The shear moduli obtained from the I_r and s_u values from the construction shown in Fig. 4 are compared with measurements from the self-boring pressuremeter at the Madingley site in Fig. 10. The cylindrical theory has again been used, and this is thought to be the more appropriate because the modulus is measured over a small strain range on elastic unloading. Both testing devices give shear moduli in the same range.

The range of I_r (Fig. 11) values is reasonable for a clay of this type, bearing in mind that it is difficult to assess the relevant strain magnitude for which G was measured.

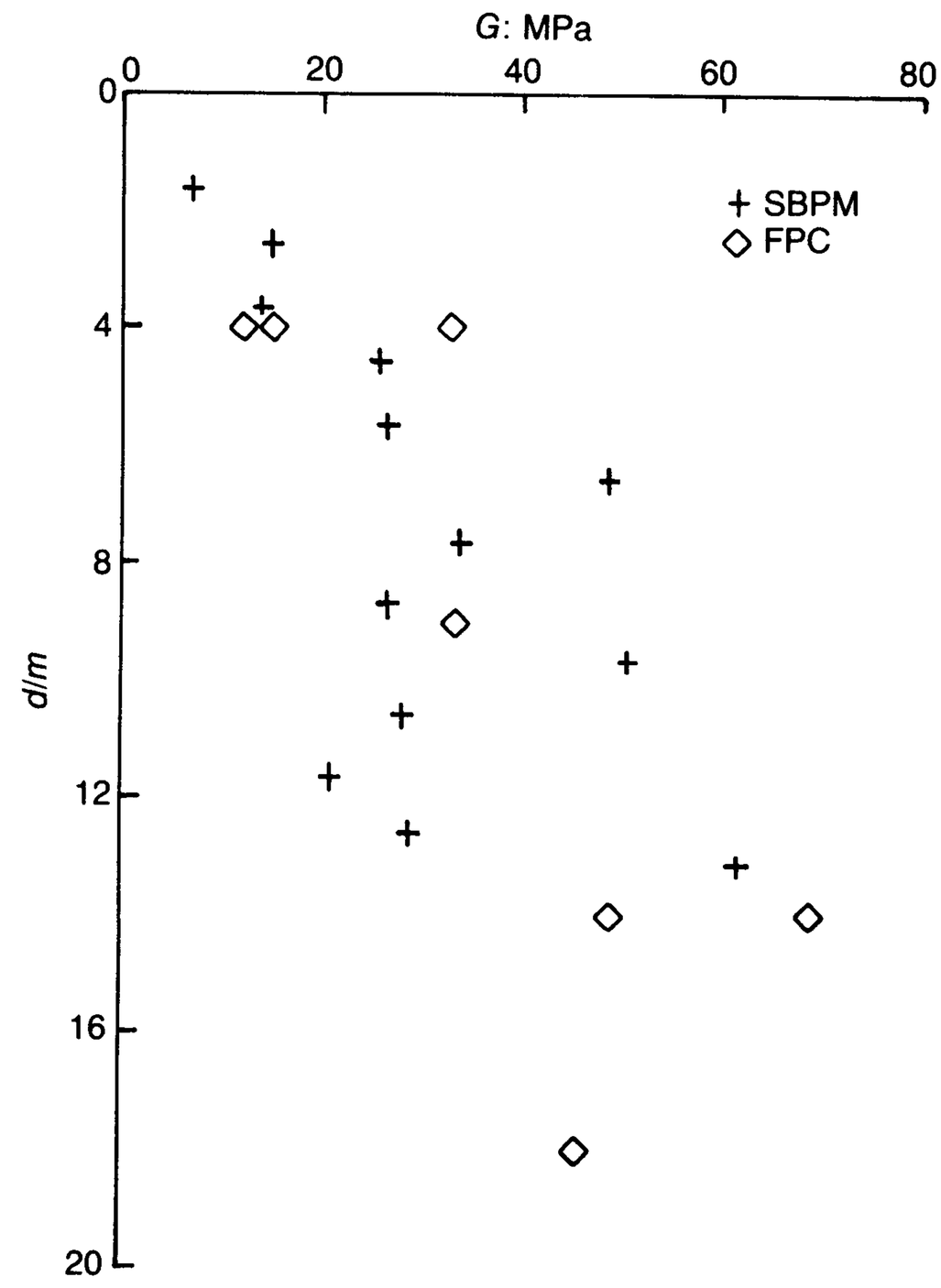

Fig. 10. Comparison of shear modulus measured by the self-boring pressuremeter (SBPM) and cone pressuremeter (FPC)

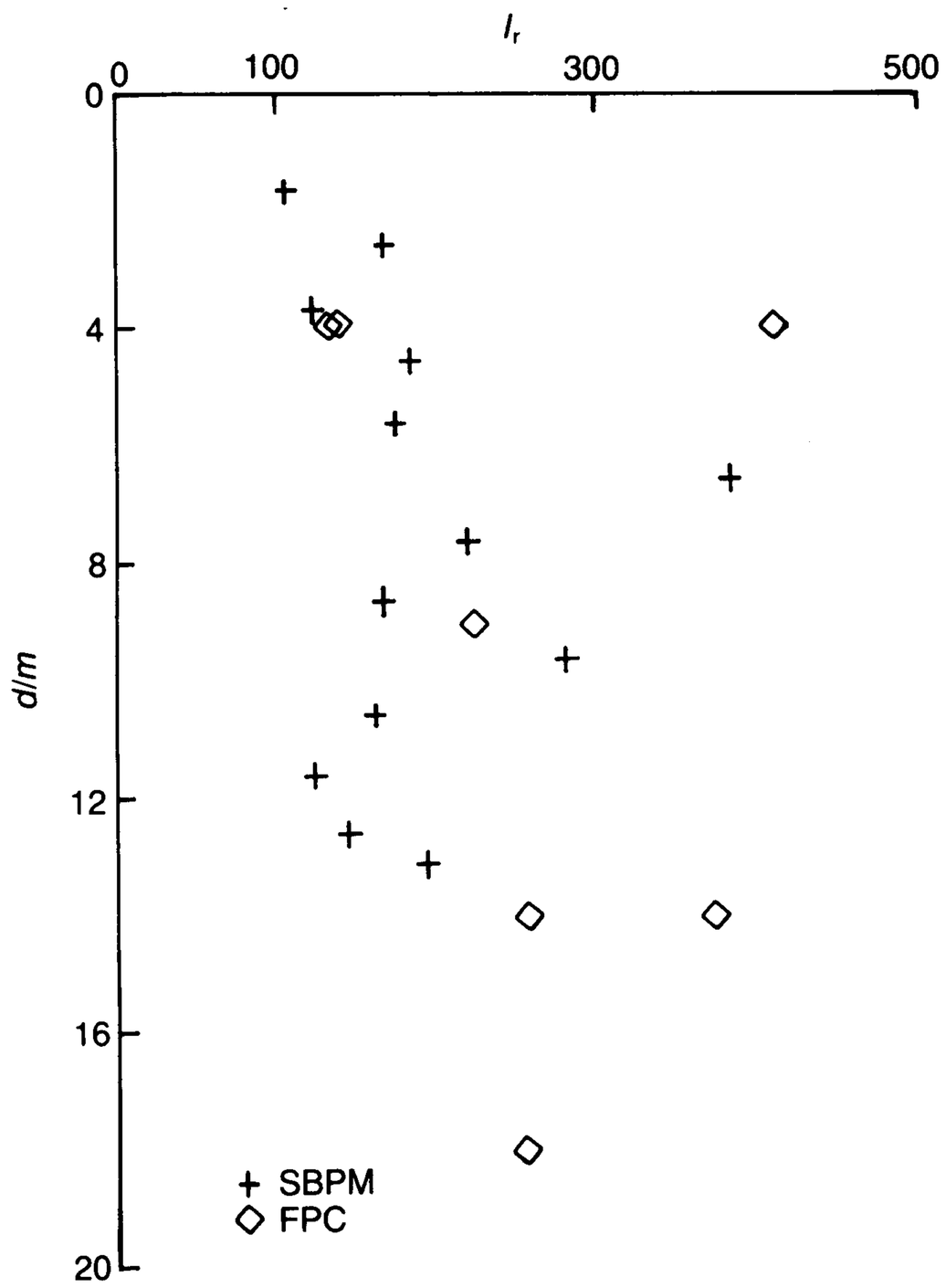

Fig. 11. Comparison of rigidity index measured by the self-boring pressuremeter (SBPM) and cone pressuremeter (FPC)

Horizontal stress

Unlike the analysis of the self-boring pressuremeter, in which the horizontal stress is assessed by examining lift-off pressures, the horizontal stress for the cone pressuremeter is obtained from the construction shown in Fig. 4. The horizontal stresses for cylindrical expansion theory shown in Table 2 imply rather high K_0 values. Estimating σ_{v0} from the bulk unit weight of the soil results in a $(\sigma_{h0} - \sigma_{v0})$ value which significantly exceeds $2s_u$ for the first test, and is therefore impossible. Of the seven tests, only the horizontal stress in test 19 (with the 2° cone tip) agreed with the previous estimates of horizontal stress from the self-boring pressuremeter (Clarke, 1979). It is clear that the interpretation using cylindrical expansion theory overestimates σ_{h0}. Lower σ_{h0} values are obtained from spherical expansion theory, and it is possible that this is more appropriate.

During installation of the long cylindrical pressuremeter, the plastically deforming region extends to a radius of $R_i(I_r)^{0.5}$ if cylindrical cavity expansion theory is assumed. During the inflation of the pressuremeter, which results in a 50% increase in radius, the elastic-plastic boundary moves out further to $1{\cdot}5R_i(I_r)^{0.5}$. With an initial length to diameter ratio of 10 and the measured I_r value of about 250, the diameter of the plastically deforming region is greater (by a factor of about 2·4) than the length of the pressuremeter. Under these circumstances it is probable that it would be more appropriate to use spherical rather than cylindrical cavity expansion theory to model the inflation.

This result should be compared with a typical self-boring pressuremeter design (Windle & Wroth, 1977) which involves a length to diameter ratio of 6 and a maximum increase in radius of 20%. This results in a plastically deforming region of radius approximately $0{\cdot}66R_i(I_r)^{0.5}$, so that even though the pressuremeter is shorter, the diameter of the plastic region is only 1·7 times the length of the pressuremeter (although even this value should cast some doubt on the interpretation using cylindrical expansion theory). It is clear that, for comparable behaviour, full-displacement pressuremeters need to have considerably longer L/D ratios than self-boring devices.

It is difficult to assess the impact of the above discussion on the initial portion of the unloading curve, for which the cylindrical theory is probably more appropriate. Detailed two-dimensional analysis using, for example, the finite element method, is required if these problems are to be solved. It is possible that the lift-off pressure may correspond more closely to the cylindrical limit pressure, and that the initial upwards curve of the pressure expansion graph is associated with a transition from approximately cylindrical to spherical conditions.

In the light of this discussion, the expansion limit pressure may be assessed as the spherical limit pressure, and the initial rising portion of the expansion curve interpreted as the rise from the cylindrical to spherical limit pressure. Using the same s_u and I_r values (i.e. not altering the interpretation of the unloading) new values of σ_{h0} can be derived. These are generally unrealistically low, indicating that in fact the expansion pressure is somewhere between the cylindrical and spherical values. The scatter of the implied horizontal stresses derived by either of these methods at any particular depth indicates, however, that at present the cone pressuremeter does not give a reliable indication of horizontal stress. This is not surprising in view of the disturbance caused by the insertion of the pressuremeter.

CONCLUSIONS

A method of analysis has been developed for full-displacement pressuremeters in clay soils. The analysis has been applied to the results of seven tests obtained with a prototype cone pressuremeter, and values of s_u, G and σ_{h0} have been derived. The analytical expression fits the unloading curve for the pressuremeter remarkably well.

A comparison of the strength and stiffness values obtained from the tests, with other test data at the same site shows that, if cylindrical cavity contraction theory is used for the interpretation of the unloading phase of the test, then the parameters derived are in good agreement with other measurements. The values of horizontal stress implied by the analysis of the expansion limit pressure indicate, however, that the cylindrical expansion theory must be in error in this case. Spherical expansion theory may be more appropriate, but a more detailed examination of the problem is required.

The cone pressuremeter is a new in situ testing device which shows clear promise for the rapid measurement of undrained strength and shear stiffness.

ACKNOWLEDGEMENTS

The Authors are grateful to Dr A. E. Organ, Research Assistant at Oxford University supported by the SERC, for checking much of the theoretical section, and to Dr J. M. O. Hughes for his continuing interest in this project. They also wish to thank J. C. P. Dalton of Cambridge Insitu for his assistance with the field work.

REFERENCES

Baguelin, F., Jezequel, J. F., Lemee, E. & Le Mehaute, A. (1972). Expansion of cylindrical probes in cohesive soils. *J. Soil Mech. Fdn Engng Div. Am. Soc. Civ. Engrs* **98,** SM11, 1129–1142.

Baligh, M. M. (1986). Undrained deep penetration I: shear stresses; II: pore pressure. *Géotechnique* **36,** No. 4, 471–501.

Brown, P. T. (1985). *Predicting laterally loaded pile capacity using the pressurementer*. MASc thesis, University of British Columbia.

Clarke, B. G. (1979). *Results of self-boring pressuremeter tests*. PMIT Report T7/R1, Cambridge University.

Fugro Ltd. (1979). *Site investigation report*. Project No. U0390-2, Cambridge University.

Gibson, R. E. & Anderson, W. F. (1961). In situ measurement of soil properties with the pressuremeter. *Civ. Engng Public Works Rev.* **56,** 615–618.

Houlsby, G. T., Clarke, B. G. & Wroth, C. P. (1986). Analysis of the unloading of a pressuremeter in sand. *Proc. 2nd Int. Symp. The Pressuremeter and Its Marine Applications*. Special Technical Publication 950. New York: ASCE.

Jezequel, J. F., Lamy, J. L. & Perrier, M. (1982). The LPC-TLM pressiopenetrometer. *Proc. Symp. on pressuremeter and marine applications, Paris*. Paris: Editions Technip.

Kay, J. N. & Parry, R. H. G. (1982). Screw plate tests in a stiff clay. *Ground Engng* **15,** 22–30.

Ladanyi, B. (1972). In situ determination of undrained stress–strain behaviour of sensitive clays with the pressuremeter. *Can. Geotech. J.* **9,** 313–319.

Norbury, J. & Wheeler, A. A. (1987). On the penetration of an elastic–plastic material by a slender body. *Q. J. Mech. Appl. Math.* **40,** No. 4, 477–491.

Palmer, A. C. (1972). Undrained plain strain expansion of a cylindrical cavity in clay: a simple interpretation of the pressuremeter test. *Géotechnique* **22,** No. 3, 451–457.

Randolph, M. F., Carter, J. P. & Wroth, C. P. (1979). Driven piles in clay—the effects of installation and subsequent consolidation. *Géotechnique* **29,** No. 4, 361–393.

Robertson, P. K., Hughes, J. M. O., Campanella, R. G. & Sy, A. (1983). Design of laterally loaded displacement piles using a driven pressuremeter, *Proc. Int. Symp. Design and Performance of Laterally Loaded Piles and Pile Groups*. Special Technical Publication 835. New York: ASCE.

Robertson, P. K., Hughes, J. M. O., Campanella, R. G., Brown, P. & McKeown, S. (1986). Design of laterally loaded piles using the pressuremeter. *Proc. 2nd Int. Symp. The Pressuremeter and Its Marine Applications*. Special Technical Publication 950. New York: ASCE.

Teh, C. I. (1987). *An analytical study of the cone penetration test*. DPhil thesis, University of Oxford.

Teh, C. I. & Houlsby, G. T. (1988). Analysis of the cone penetration test by the strain path method. *Proc. 6th Int. Conf. Num. and Analy. Meth. in Geomech., Innsbruck* **1,** 397–402.

Vesic, A. S. (1963). Bearing capacity of deep foundations on sand. *Stresses in soils and layered systems*. Canadian Highway Research Board, Report 39.

Windle, D. & Wroth, C. P. (1977). The use of the self-boring pressuremeter to determine the properties of clays. *Ground Engng* **10,** No. 1, 37–46.

Withers, N. J., Schaap, L. H. J. & Dalton, C. P. (1986). The development of the full displacement pressuremeter. *Proc. 2nd Int. Symp. The Pressuremeter and Its Marine Applications*. Special Technical Publication 950. New York: ASCE.

Wroth, C. P. (1984). The interpretation of in situ soil tests. *Géotechnique* **34,** No. 4, 447–492.